

# Real and Reciprocal Space Characterization of the 3-Dimensional Charge Density Wave in Quasi-1-Dimensional CuTe

Fei Guo<sup>1,2</sup>, Michele Puppini<sup>1,2</sup>, Lukas Hellbrück<sup>1,2</sup>, Arnaud Magrez<sup>1</sup>,  
Eduardo B. Guedes<sup>3</sup>, Igor Sokolović<sup>4</sup>, and J. Hugo Dil<sup>1,2,3</sup>

<sup>1</sup>*Institute of Physics, École Polytechnique Fédérale  
de Lausanne, CH-1015 Lausanne, Switzerland*

<sup>2</sup>*Lausanne Centre for Ultrafast Science (LACUS),*

*École Polytechnique Fédérale de Lausanne (EPFL), CH-1015 Lausanne, Switzerland*

<sup>3</sup>*Photon Science Division, Paul Scherrer Institut, CH-5232 Villigen, Switzerland*

<sup>4</sup>*Institute of Applied Physics, Technische Universität Wien, 1040 Vienna, Austria*

(Dated: May 16, 2024)

# Abstract

Low-dimensional materials are susceptible to electronic instabilities such as charge density waves (CDWs), originating from a divergence in the Lindhard electron response function, combined with a finite electron-phonon coupling strength. In this report, we present a detailed characterisation of the CDW in the quasi-one-dimensional material CuTe, including (1) direct visualization of lattice distortion seen with non-contact atomic force microscopy in real space, (2) the out-of-plane momentum dependency of the CDW gap size of the quasi-1-dimensional bands, by angle-resolved photoemission spectroscopy, (3) coherent dynamics of a photoexcited phonon mode seen by time- and angle-resolved photoemission spectroscopy, with frequency and wavevector  $\mathbf{q}_{\text{CDW}}$  corresponding to the soft phonon modes predicted by theory. Furthermore, we find that the CDW gap closes through a transient band renormalisation. We thus confirm that, despite the quasi-1D characteristics of CuTe, it hosts inherently 3-dimensional CDWs.

## I. INTRODUCTION

Low-dimensional materials are a vibrant field of research due to their rich number of competing broken symmetry ground states [1, 2], which are promising for novel electronic functionalities [3, 4] and the possibility of ultrafast optical manipulation [5]. An ubiquitous effect is the susceptibility to charge ordering instability, such as charge density waves (CDWs). In the past few decades, there have been great efforts to understand the driving mechanisms of several CDW-hosting systems [6], for example, quasi-2D transition metal dichalcogenides (TMDCs) [7, 8], rare-earth tritellurides ( $RTe_3$ s) [9, 10], as well as in quasi-1D systems [11, 12]. The formation of CDWs can be due to an electronic instability driven by Fermi surface nesting [13, 14], combined with electron-phonon coupling [15, 16]. Electron-electron couplings are believed to be the driving force for CDW in different scenarios, for example in excitonic insulators [17], or via the band Jahn-Teller effect [18]. In reality, CDWs are likely to arise due to an interplay between multiple of the above factors, which cannot be easily individually resolved. The characterization of materials hosting CDWs requires a quantitative evaluation of the direction and periodicity of charge density modulation represented by the CDW wavevector  $\mathbf{q}_{\text{CDW}}$ , along with the energy scale of such modulation in the form of a transition temperature  $T_{\text{CDW}}$ , or the magnitude of the energy gap, as well as a case-specific evaluation of the driving many-body couplings.

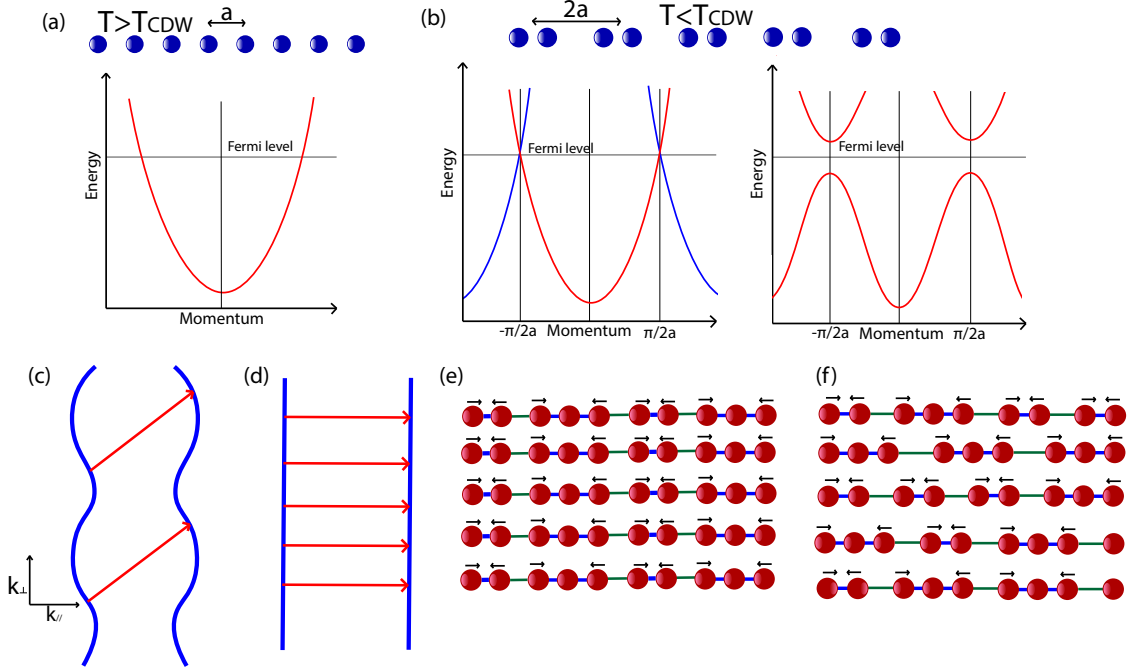


FIG. 1: Schematic drawing of (a) undistorted and (b) Peierls distorted lattices and electronic band dispersion; Fermi surface nesting of (c) 3D and (d) 1D CDWs in the first definition in terms of  $\mathbf{q}_{CDW}$  [20], with Fermi surface (blue) and nesting wavevector  $\mathbf{q}_{CDW}$  (red); lattice distortions of (e) 3D and (f) 1D CDWs in the second definition in terms of inter-layer collectivity [12].

In this report, we present an investigation of the quasi-1D CDW material copper telluride (CuTe) [19]. We first directly visualize the spatial charge ordering modulations via non-contact atomic force microscope (ncAFM), then, we measure with angle-resolved photoemission spectroscopy (ARPES) the electronic band dispersion of CuTe, including the dispersion orthogonal to the surface plane  $k_z$ . Our data reveals a  $k_z$ -dependent gap, together with evidence of inter-layer couplings in the ordering of the CDW. Finally we investigate electron-phonon coupling in the system by femtosecond time-resolved ARPES (trARPES), showing coherent oscillation of specific location of the band structure. The oscillation correspond to a soft phonon mode linked to the CDW, but are strongly coupled with inherently 3D states at the Fermi surface. Further, we can follow the ultrafast closing of the CDW gap through a renormalisation of the quasi 1D bands. In light of these results, we discuss the dimensionality of the CDW in CuTe and show that under all typical definitions of dimensionality the CDW in CuTe is 3-dimensional, despite the fact that both the atomic and electronic structures show remarkable quasi-1D features.

In the simplest model, the formation of a CDW in quasi-1D materials follows a Peierls

scenario, in which pairs of atoms dimerize. This modulation overcomes Coulomb repulsion by opening up a gap at the Fermi energy and hence lowering the total energy in the system. The formation of this superstructure introduces an additional periodicity and ‘replica’ bands, as shown in Fig.1(a) and (b). In this model, the Lindhard response function  $\chi(\mathbf{q})$  is a key parameter:

$$\chi(\mathbf{q}) = \sum_k \frac{f(\epsilon_k) - f(\epsilon_{k+q})}{\epsilon_k - \epsilon_{k+q}} \quad (1)$$

Here  $\mathbf{q}$  is the electron wavevector,  $\epsilon_k = \frac{\hbar^2 k^2}{2m}$  is the electron’s kinetic energy, and  $f(\epsilon_k)$  is the Fermi-Dirac distribution.  $\chi'(\mathbf{q})$  diverges whenever  $\epsilon_k = \epsilon_{k+q}$ , i.e. two parts of the Fermi surface are connected by a wavevector  $\mathbf{q}$ , a condition referred to as Fermi surface nesting. In the case of a strictly 1D system, the real part of  $\chi(\mathbf{q})$  can be expressed as  $\chi'(\mathbf{q}) = \frac{1}{q} \ln \left| \frac{q-2k_F}{q+2k_F} \right|$  and has a weak divergence at  $q = \pm 2k_F$  [21]. This susceptibility renormalizes the phonon frequency  $\omega_q$  to:

$$\omega_{ren,q}^2 = \omega_q^2 + \frac{2g^2\omega_q}{\hbar}\chi(q, T) \quad (2)$$

Where  $g$  is the electron-phonon coupling constant [22]. With finite electron-phonon coupling, the renormalized phonon frequency  $\omega_{ren,q}$  shows a sharp dip at divergence of  $\chi'(\mathbf{q})$ , and this indicates an instability of the lattice structure and a tendency to charge density reordering. However, the divergence of  $\chi'(\mathbf{q})$  is not protected with respect to carrier scattering and small geometrical deviations from perfect nesting conditions [21]. Given this fact, one might expect that CDWs could only survive in quasi-1D systems with nearly perfect nesting, but there is plenty of evidence that CDWs exist in 2D [23–25] and even 3D [26, 27] systems. Therefore, Fermi Surface nesting and electron-phonon coupling are certainly not the only mechanism of CDW formation for higher-dimensional materials.

The dimensionality of CDWs in low-dimensional materials is widely discussed in the literature, but not uniquely defined. For instance, some authors define a 3-dimensional CDW as one where the CDW-associated lattice distortion is not purely in-plane, and, as shown in Fig.1(c), there is a finite out-of-plane component of the CDW wavevector  $\mathbf{q}_{CDW}$  [20]. Thus a 1-dimensional CDW in this picture would correspond to a 1D Fermi surface with a nesting wavevector  $\mathbf{q}_{CDW}$  purely along one in-plane direction (Fig.1(d)). Other authors define a 3-dimensional CDW where all layers in the material have the same  $\mathbf{q}_{CDW}$  and modulate coherently, but  $\mathbf{q}_{CDW}$  itself does not need an out-of-plane component [12].

A 1-dimensional CDWs in this picture would be an individual modulation on each atomic chain without any inter-layer collectivity, despite having the same  $\mathbf{q}_{\text{CDW}}$ . This distinction is shown schematically in Fig.1(e) and (f). At this point, it is worth mentioning that a purely 1D system cannot sustain stable long-range orders due to quantum and thermal fluctuations, and inter-layer collectivity is a prerequisite to the formation of charge and spin density waves [28, 29].

The subject of this article, CuTe, is a quasi-1D material, with the atomic structure shown in Fig.2(a) [30], which has been reported to undergo a CDW phase transition at 335 K. The electronic band structure of CuTe has been investigated with ARPES [19], revealing a momentum-dependent gap as large as 190 meV which forms along quasi-1d Fermi surface sheets. The static electronic band structure and the CDW gap were reported as a function of temperature and doping, to visualize the closure of the gap. First-principle calculations of the phonon spectrum were also presented showing soft phonon modes at the observed nesting wavevector, which also corresponds to maxima of the calculated electron scattering susceptibility. These results thus indicate that electron-phonon coupling and Fermi surface nesting indeed contribute dominantly to the formation of the CDW in CuTe. Recently, detailed electronic structure and ultrafast nonequilibrium carrier dynamics near the Brillouin zone center of CuTe has also been studied with low-photon-energy ARPES and trARPES [31]. In this work, we expand on those results and elucidate the dimensionality of the CDW in CuTe, by providing both real and reciprocal space investigations.

## II. METHODS

High quality single crystals of CuTe were synthesized using the flux technique. A mixture of Cu and Te (atomic ratio 1:20) was sealed under vacuum within a quartz ampoule. This ampoule was then placed in a vertical furnace and heated to  $600\hat{\text{A}}^\circ\text{C}$ , where it remained for 12 hours before being gradually cooled to  $450\hat{\text{A}}^\circ\text{C}$  at a cooling rate of  $10\hat{\text{A}}^\circ\text{C}$  per hour, and then further cooled to  $325\hat{\text{A}}^\circ\text{C}$  at a slower rate of  $1\hat{\text{A}}^\circ\text{C}$  per hour. Following the crystal growth process, the resulting crystals in the solidified Te flux were transferred in a quartz tube furnace and maintained at  $270\hat{\text{A}}^\circ\text{C}$  under dynamic vacuum. After the complete removal of the Te flux by sublimation, golden CuTe crystals were obtained. The structure and stoichiometry were confirmed by single-crystal diffraction and X-ray fluorescence spectroscopy.

Non-contact atomic force microscopy (ncAFM) measurements were performed using a Omicron qPlus low-temperature head mounted in an ultrahigh vacuum (UHV) chamber. Stiff qPlus sensors [32] ( $k = 1800 \text{ N}\cdot\text{m}^{-1}$ ,  $Q=5000\text{--}30000$ ,  $f_0 \in [25\text{--}45] \text{ kHz}$ ) with a sharp W tip [33] were used for imaging. Cantilever deflection was supported with an in-vacuum cryogenic preamplifier [34]. Prior to cleaving a CuTe sample and imaging the cleaved surface, sharp W tips were additionally decorated with a sharp Cu pyramid at the apex by deliberate tip restructuring on a Cu(110) surface. Damping of external vibrations was assisted by suspending the whole chamber with 36 bungee cords [35].

Single-crystal CuTe samples were prepared by attaching them to standardized sample plates and attaching a stainless steel top post using conductive silver epoxy. The silver epoxy was cured by baking this structure at  $80^\circ\text{C}$  for 4 hours in ambient air. Samples were cleaved at room temperature in a chamber with an UHV base pressure below  $1 \times 10^{-10}$  mbar, quickly transferred *in – situ* to a separate chamber with the base pressure below  $1 \times 10^{-11}$  mbar where they were introduced to the measurement head and subsequently imaged at  $T = 5 \text{ K}$ . Such treatment of cleaved surfaces results in a negligible amount of adsorbates, even on much more reactive surfaces [36].

For ARPES measurements samples were prepared in the same way as for the ncAFM measurement. For the  $k_z$  resolved ARPES measurements samples were cleaved in-situ in ultrahigh vacuum below  $5 \times 10^{-10}$  mbar and at  $T = 24 \text{ K}$ , and for the trARPES measurements samples were cleaved in-situ in ultrahigh vacuum at  $T = 70 \text{ K}$ . High-resolution ARPES measurements as a function of photon energy were taken at the SIS-ULTRA beamline of the Swiss Light Source, Paul Scherrer Institut. All band structures were measured with circular  $C+$  polarized light. trARPES measurement were taken at the LACUS facility at the EPFL [37], which has a high-harmonic generation (HHG) source of extreme ultraviolet (XUV) laser, along with an infra-red pump laser of wavelength  $780 \text{ nm}$  (photon energy  $1.6 \text{ eV}$ ), which provides a time resolution better than  $100 \text{ fs}$ . trARPES data were collected with  $p$ -polarized HHG light with a photon energy of  $40.35 \text{ eV}$ .

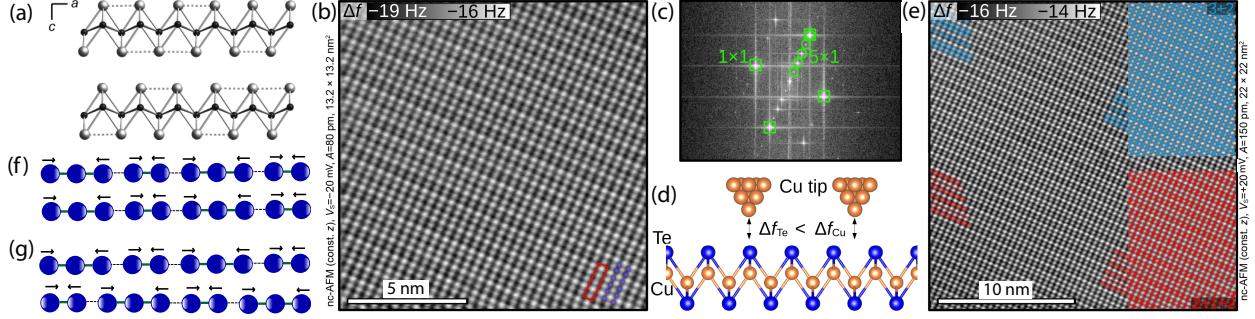


FIG. 2: (a) atomic structure of modulated CuTe, each Cu(black) is coordinated with 4 Te(grey) atoms, 2 or 3 Te atoms group together in the CDW state [30](b) small area detailed image: Te atoms are imaged as dark spheres (attraction) while white spheres indicate absence of atoms (only long-range forces). Te atoms are highlighted as blue spheres and the  $5 \times 1$  repeat unit cell is indicated in red. (c) fast Fourier transform of ncAFM image, with  $5 \times 1$  reconstruction in one direction and only  $1 \times 1$  peaks in the perpendicular direction, (d) schematic drawing of the atomic structure of CuTe and ncAFM contrast formation: Surface-terminating Te atoms act with chemical attraction (negative  $\delta f$ ) towards the Cu-terminated tip, while the Cu atoms below the surface primarily contribute with long-range van der Waals forces ( $\delta f$  closer to zero), (e) ncAFM image on extended area, with 2 domains of CDWs with periodicities  $2 + 1 + 2$ (red) and  $3 + 2$ (blue) respectively; schematic drawing of two different bilayer arrangements of the distorted atomic chain: (f)  $3+2$  on  $3+2$ , and (g)  $3+2$  on  $2+3$ .

### III. PERIODIC LATTICE DISTORTION: DIRECT EVIDENCE OF CDW IN CUTE

The crystal structure of CuTe is shown in Fig.2(a), the 1d nature is reflected by the appearance of chains of Cu atoms, each coordinated with 4 Te atoms. Non-contact atomic force microscopy (ncAFM) was used to visualize the real space CDW. A topographic image of a high-quality surface is shown in Fig.2(b). The surface is seen to undergo a  $5 \times 1$  lattice modulation, as more clearly observed by a fast Fourier transform in Fig.2(c) which shows a unidirectional  $5 \times 1$  reconstruction. However, as shown by an ncAFM image of a larger area in Fig.2(e), the CDW modulation is not simply  $5 \times 1$ , but proceed either as  $2 + 1 + 2$  (red in Fig.2(e)) or  $3 + 2$  (blue in Fig.2(e)) modulations, forming small domains coexisting on a patch of  $20 \times 20 \text{ nm}^2$ .

The modulation wavevector of the CDW is  $\mathbf{q}_{\text{CDW}} = (0.4\mathbf{a}^*, 0\mathbf{b}^*, \frac{1}{2}\mathbf{c}^*)$ , in which  $\mathbf{a}^*$  is the reciprocal lattice vector in the chain direction, and  $\mathbf{c}^*$  is the reciprocal lattice vector in the out-of plane direction [30]. The magnitude of the  $\mathbf{c}^*$  component of  $\mathbf{q}_{\text{CDW}}$  is dictated by the orthorhombic point group symmetry [38]. Therefore, in reality we should expect

an actual superstructure with a thickness of 2 layers. This could potentially explain the structure of the 2 + 1 + 2 domains seen in Fig.2(e). In order for  $\mathbf{q}_{\text{CDW}}$  to overlap with the reciprocal lattice vectors, it needs to be multiplied by 2 in the  $\mathbf{c}^*$  direction and 2.5 in the  $\mathbf{a}^*$  direction. For a commensurate CDW, a superstructure with 2.5 lattice sites is not possible, so the lattice reconstructs with either 2 or 3 sites, alternating to finally form a periodicity of 5 lattice sites. Then, the periodicity of 2 in the  $\mathbf{c}^*$  direction comes into play: the 3 + 2 superstructure has broken inversion symmetry, so there are 2 nonequivalent arrangements of 2 layers, 3 + 2 on 3 + 2, or 3 + 2 on 2 + 3. These are shown schematically in Fig.2(f) and (g). With the 3 + 2 on 2 + 3 arrangement, the ncAFM tip can detect different modulations on the 2 topmost layers, appearing like a 2 + 1 + 2 modulation.

Given this 3-dimensional superstructure in real space, it is then instructive to explore the electronic band dispersion in 3-dimensional reciprocal space.

#### IV. ELECTRONIC BAND DISPERSION OF CUTE

ARPES is the most direct way to visualize the electronic band structure, where the onset of a CDW state is characterized by the opening of a band gap. The Fermi surface of CuTe probed by ARPES is shown in Fig.3(a), which shows a central feature extending in the  $k_x$  direction, and 2 quasi-1D bands extending in the  $k_y$  direction [19]. In the CDW state, these bands display a  $k_y$ -dependent gap, with a maximum of 190 meV at  $k_y = 0.3 \text{ \AA}^{-1}$ . Here we investigate the  $k_z$ -dependence of the band structure, by tuning the photon energy.

We first focus on the cut  $k_y = 0$ , the band structure of which is shown in Fig.3(b), and vary the photon energy from 41 eV to 93 eV, with a step of 2 eV. The resulting  $k_z$  dispersion is shown in Fig.3(d). It is clear that the bands at  $k_y = 0$  disperse strongly along the  $k_z$  direction and thus have a 3D nature, as also expected from calculations [30]. A similar procedure was carried out for the cut at  $k_y = 0.4 \text{ \AA}^{-1}$  across the quasi-1D bands, the dispersion of which is shown in Fig.3(c). To stay at a constant  $k_y$  value, the tilt angle  $\theta$  was adjusted at each photon energy according to the relationship  $k_y = \frac{\sqrt{2mE_k}}{\hbar} \sin \theta$ . The obtained dispersion is shown in Fig.3(e). These bands barely show any dispersion as a function of  $k_z$ , and have therefore indeed a clear quasi-1D character. The band maximum is shown in Fig.3(f), and displays a periodic variation in  $h\nu$ . The CDW gap size was extracted for each photon energy and plotted as a function of the calculated  $k_z$  in Fig.3(g), with an inner potential of 9.5 eV

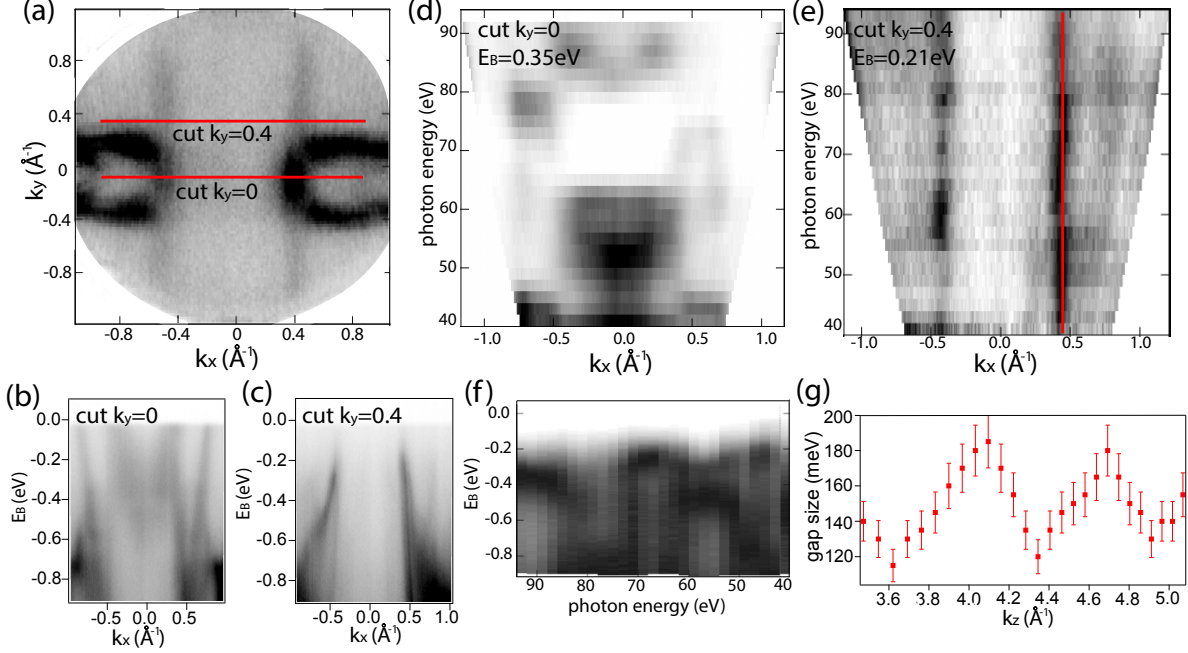


FIG. 3: (a) constant binding energy dispersion of CuTe taken at  $h\nu = 65$  eV, the  $k_y$  values at which  $h\nu$  scans were performed are marked with red lines, (b) band map taken at  $k_y = 0 \text{ \AA}^{-1}$ , with  $h\nu = 65$  eV, (c) band map taken at  $k_y = 0.4 \text{ \AA}^{-1}$ , with  $h\nu = 65$  eV, (d)  $h\nu$  dependency at  $k_y = 0 \text{ \AA}^{-1}$  showing a clear dispersion, indicating 3D nature of the bands, (e)  $h\nu$  dependency at  $k_y = 0.4 \text{ \AA}^{-1}$ , the bands are not dispersing in  $k_z$ , indicating their 1D nature, (f) energy distribution as a function of photon energy for  $k_y = 0.4 \text{ \AA}^{-1}$  and  $k_x = 0.46 \text{ \AA}^{-1}$  marked in (e), (g) CDW gap size variation with  $k_z$

extracted from the  $h\nu$  periodicity of the 3D bands in Fig.3(d). The difference in  $k_z$  between the 2 gap size maxima in Fig.3(g) is  $0.59 \text{ \AA}^{-1}$ . The observed periodicity of the CDW gap along the  $k_z$  direction further supports the 3D nature of the CDW.

The above results indicate that CuTe hosts 3-dimensional CDWs in terms of the modulation wavevector  $\mathbf{q}_{CDW}$ , which has a finite component in the z-direction. Also, the prerequisite of inter-layer collectivity to the formation of CDWs, and the absence of Luttinger liquid-like behaviour [39] suggests that all the layers modulate collectively at low temperatures, hence the CDW is 3D inherently according to the second definition. Overall, we find that at temperatures well below  $T_{CDW} = 335$  K, CuTe, albeit quasi-1D, hosts 3-dimensional CDWs with respect to both common definitions.

## V. COHERENT DYNAMICS OF CUTE

Electron-phonon coupling is a critical ingredient in the CDW-forming mechanism, here we investigate it by observing the coherent dynamics of the band structure, initiated by a short optical perturbation. Through the oscillation of the electronic bands, one can find the frequencies associated to strongly coupled phonon modes that drives the Fermi surface nesting. For this purpose, pump-probe time-resolved ARPES (trARPES) is a powerful tool, as it can identify directly coupling to specific bands with momentum resolution [40, 41].

To that end, we performed trARPES in our LACUS facility [37]. In this experiment, 1.6 eV pump infrared laser pulses were used to excite electrons to states above the Fermi level, then, after an adjustable time delay, an extreme ultraviolet (XUV) laser of 40.35 eV photon energy was used to probe the band structure by photoemission. Fig.4(a) demonstrates a time delay difference spectrum measured by this technique: red denotes positive signal, corresponding to an increased intensity at a time delay of 100 fs compared to negative time delays (probe before the pump), and blue denotes an intensity decrease. In Fig.4(a), the red area with kinetic energy  $\geq 36.4$  eV indicates excited states above the Fermi level. Since the bands cross the Fermi level, the excited states at high kinetic energies relax quickly following an exponential decay with  $\tau \approx 730$  fs, as shown in Fig.4(b).

We first focus on the bands at  $k_x = -0.34 \text{ \AA}^{-1}$  in reciprocal space, as marked on the schematic Fermi surface in Fig.4(c). According to Fig.3(b), these bands show strong 3D characteristics. The corresponding band map is shown in Fig.4(d). We follow the intensity evolution in an area close to the Fermi level, marked in Fig.4(e). Clear oscillation of intensity can be seen, and the time distribution of intensity can be fitted with a multi-exponential decay with decay time of  $2110 \pm 120$  fs and oscillation frequency  $f \approx 2.06 \pm 0.1$  THz, which corresponds to  $69 \pm 3 \text{ cm}^{-1}$ . Another way to observe these oscillations is to track directly the movement of bands as a function of pump-probe time delay. Fig.4(f) shows the momentum distribution of intensity at a constant kinetic energy directly below the Fermi level with varying time delays. The maximum of the momentum intensity distribution at negative  $k_y$  was extracted as a function of time delay in Fig.4(g), on which similar oscillations were fitted with a decay time of  $1520 \pm 120$  fs and oscillation frequency of  $f \approx 2.32 \pm 0.2$  THz, which corresponds to a phonon frequency of  $77 \pm 7 \text{ cm}^{-1}$ . The above findings indicate that with the pump laser, we have photo-excited a phonon mode of CuTe. Interestingly, *ab-*

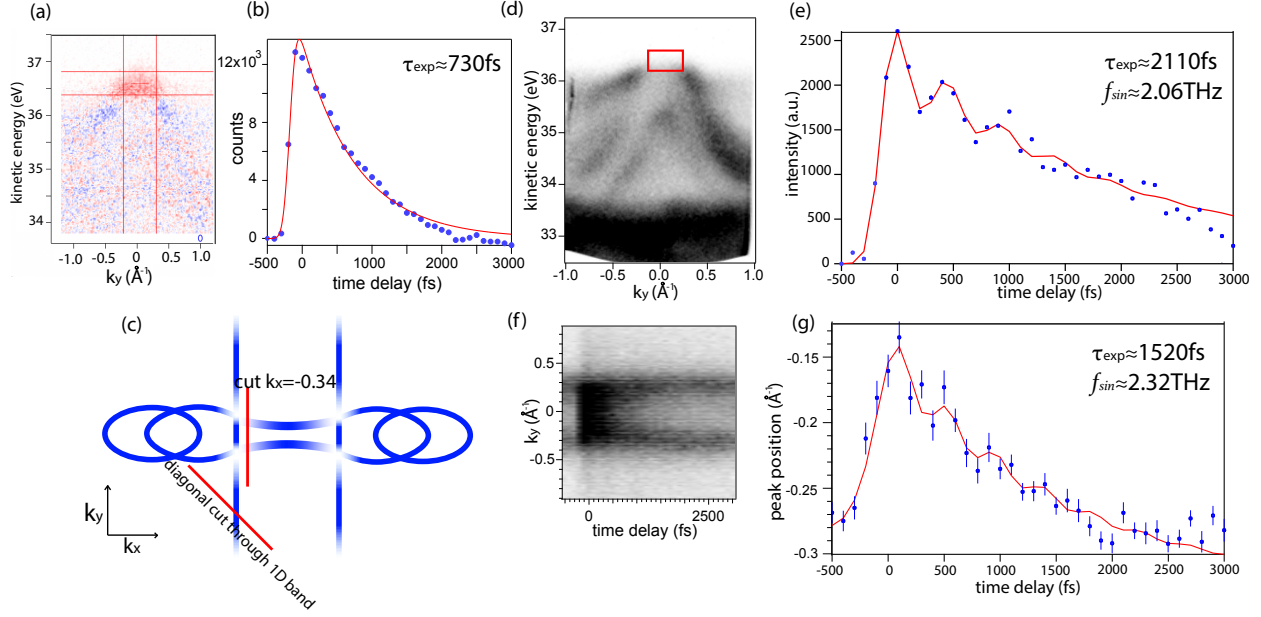


FIG. 4: (a) difference spectrum measured with trARPES at  $k_x = -0.34 \text{ \AA}^{-1}$  for a time delay of 100 fs: red denotes extra intensity compared to negative time delay, and blue denotes vanished intensity compared to negative time delay, (b) integrated intensity in marked region in (a), as a function of time delay, (c) schematic drawing of Fermi surface of CuTe, (d) bandmap with  $k_x = -0.34 \text{ \AA}^{-1}$  marked in (c), (e) time-delay distribution of intensity integrated in the area marked in (d), along with line fitting with a multi-exponential multiplied by a sinusoidal function, (f) momentum distribution of intensity at constant energy and  $k_x$  as a function of time delay, (g) time-delay distribution of the negative- $k_y$  intensity peak position from (f). All of the above are taken at photon energy  $h\nu = 40.35 \text{ eV}$ .

*initio* calculations of the phonon spectrum [19] indicate softening for two phonon modes at  $\mathbf{q} = (0.4, 0, 0)$  and  $\mathbf{q} = (0.4, 0, 0.5)$  respectively, with softened phonon frequencies in the range of  $60 - 85 \text{ cm}^{-1}$ , comparable with the observed phonon frequency. This is further evidence that the predicted soft phonon mode  $\mathbf{q}$  [19] is indeed present in CuTe.

Gap-filling dynamics has been studied extensively on CDW materials, and is often accompanied by an oscillation of in-gap intensity or gap size [42–45]. For this purpose, trARPES measurements of the 1D band were taken in a diagonal  $k_x - k_y$  direction, around the 1D band as shown by the diagonal red line in Fig.4(c), and the corresponding band map is shown in Fig.5(a). For each of the marked kinetic energies in Fig.5(a), momentum distribution of intensity is visualized as a function of time, as representatively shown for  $E_2 = 35.7 \text{ eV}$  and  $E_3 = 35.3 \text{ eV}$  in Fig.5(b). From these momentum distributions we extracted the temporal evolution of the change of the intensity peak position, as shown in Fig.5(c). To characterize

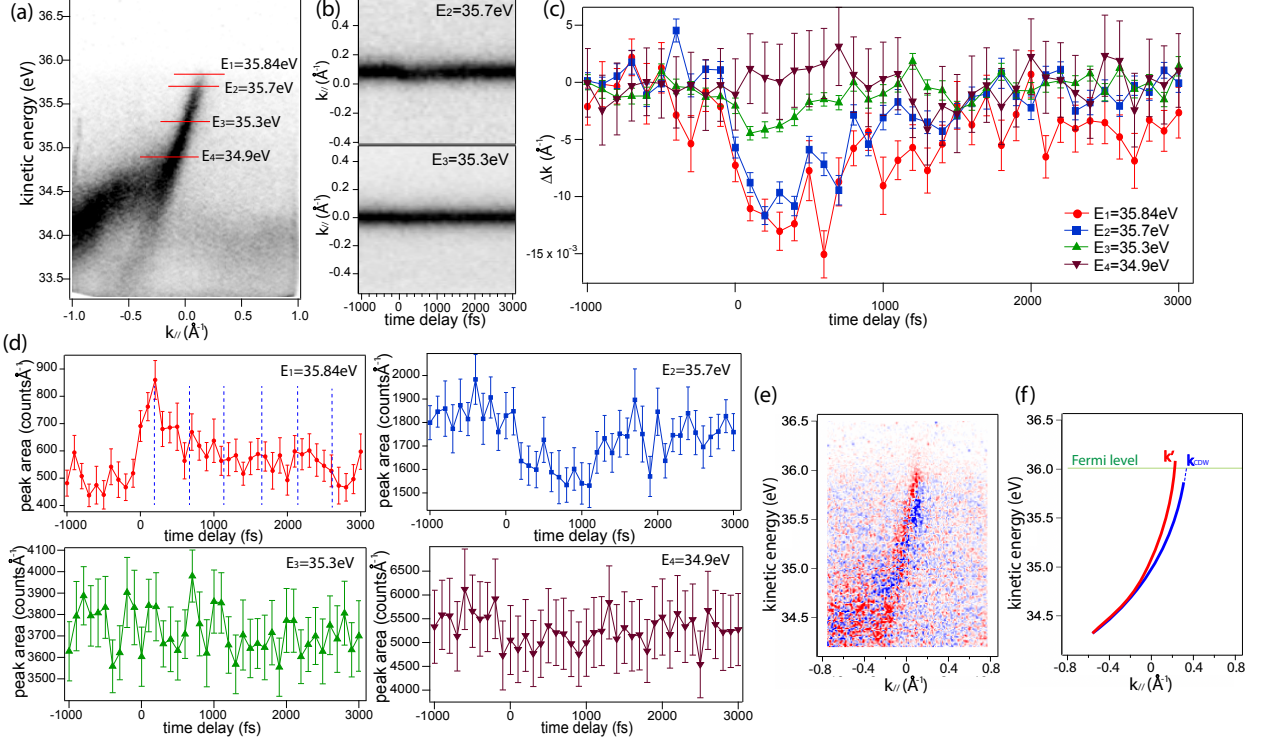


FIG. 5: (a) bandmap with diagonal  $k_{//}$  marked in Fig.4(c), (b) representative momentum distributions of intensity as a function of time delay, at kinetic energies  $E_2$  and  $E_3$  marked in (a), (c) intensity peak position change (as compared to negative time delays) as a function of time delay, at all kinetic energies marked in (a), (d) peak area as a function of time delay, at kinetic energies marked in (a) blue dashed lines stands for time period extracted from 3D band coherent oscillation in Fig.4(e), (e) Difference spectrum of quasi-1D band at time delay of 200 fs, as compared to negative time delay, (f) schematic drawing of the quasi-1D band before optical pumping (blue), and at 200 fs after optical pump arrives (red). All of the above are taken at photon energy  $h\nu = 40.35$  eV.

the intensity evolution, we calculated the peak area (= FWHM peak width  $\times$  peak intensity) for each kinetic energy, as shown in Fig.5(d). At kinetic energy  $E_1 = 35.84$  eV, which is within the CDW gap, we see a pronounced renormalization in band position and a gap filling which decays on the order of 700 fs, much shorter compared to the 2110 fs observed for the 3D bands in Fig.4(e). However, even with the oscillation periodicity of the 3D bands from Fig.4(e) superimposed, it is difficult to identify any clear oscillations within the experimental uncertainty. At kinetic energy  $E_2 = 35.7$  eV, comparable band renormalization is seen, along with an intensity depletion which recovers with a slightly longer time scale. At the 2 lower kinetic energies, we see no pronounced band renormalization or intensity change within the experimental signal to noise ratio.

The phenomenon of band renormalization upon optical excitation is expected to arise

from transiently enhanced screening by high-energy electrons and holes. It has been reported for gapless states of the nodal-line semimetal ZrSiSe [46], and for CDW-state HoTe<sub>3</sub> [45]. For the latter, enhanced screening transiently reduces the tight binding parameter  $t_{\perp}$ , and nesting conditions are improved as a result of this renormalization. On CuTe, in contrast, this screening-induced renormalization has a consequence of transient CDW melting. Fig.5(e) shows a difference spectrum taken at a time delay of 200 fs, in which we see a renormalization of the band gradient. As a result, the momentum at which the band crosses the Fermi level changes accordingly. This situation is illustrated schematically in Fig.5(f). Since the renormalized band (red) crosses the Fermi level with a momentum which slightly differs from the nesting wavevector, the nesting condition is no longer fulfilled and the CDW is transiently melted.

Overall, with our laser pump-probe trARPES experiment, we discover that, the photoresponse of the system to femtosecond excitation comprises of a coherent response to the softened phonon mode, which appear to be strongly coupled to the 3D states, and an incoherent hot electron response lasting several hundreds of femtoseconds. For the 1D states, only an incoherent dynamic was observed, associated to an ultrafast gap filling and dispersion renormalization towards worsened nesting conditions. Interestingly, the gap filling relaxation time, 700 fs, is shorter than the hot electron relaxation (around 2 ps) measured in the 3D states.

## VI. CONCLUSION

In this work, we combined different techniques and demonstrated for CuTe for the first time to our knowledge, that the real space CDW superstructure and the reciprocal space CDW gap size both have a periodicity in the out-of-plane direction. These are evidences that the CDW wavevector  $\mathbf{q}_{\text{CDW}}$  has a finite out-of-plane component. Together with the prerequisite of inter-layer collectivity for CDW formation, we confirm that the CDW in this quasi-1D material is 3D by all definitions. Our results reveal that interlayer coupling effects play an important role in the CDW of CuTe, and highlight the importance of combining multiple experimental probes.

## ACKNOWLEDGEMENT

F.G. and J.H.D. acknowledge support from the Swiss National Science Foundation (SNSF) Project No. 200021-200362

---

- [1] A. F. Young, J. D. Sanchez-Yamagishi, B. Hunt, S. H. Choi, K. Watanabe, T. Taniguchi, R. C. Ashoori, and P. Jarillo-Herrero, *Nature* **505**, 528 (2014).
- [2] S. S. Hegde and I. S. Villadiego, *Phys. Rev. B* **105**, 195417 (2022).
- [3] W. Ahmad, Y. Gong, G. Abbas, K. Khan, M. Khan, G. Ali, A. Shuja, A. K. Tareen, Q. Khan, and D. Li, *Nanoscale* **13**, 5162 (2021).
- [4] J. M. Kim, M. F. Haque, E. Y. Hsieh, S. M. Nahid, I. Zarin, K.-Y. Jeong, J.-P. So, H.-G. Park, and S. Nam, *Advanced Materials* **35**, 2107362 (2023).
- [5] A. O. Slobodeniuk, P. Koutenský, M. Bartoš, F. Trojánek, P. Malý, T. Novotný, and M. Kozák, *npj 2D Materials and Applications* **7**, 17 (2023).
- [6] X. Zhu, Y. Cao, J. Zhang, E. W. Plummer, and J. Guo, *Proceedings of the National Academy of Sciences* **112**, 2367 (2015), <https://www.pnas.org/doi/pdf/10.1073/pnas.1424791112>.
- [7] S. V. Borisenko, A. A. Kordyuk, A. N. Yaresko, V. B. Zabolotnyy, D. S. Inosov, R. Schuster, B. Büchner, R. Weber, R. Follath, L. Patthey, and H. Berger, *Phys. Rev. Lett.* **100**, 196402 (2008).
- [8] S. V. Borisenko, A. A. Kordyuk, V. B. Zabolotnyy, D. S. Inosov, D. Evtushinsky, B. Büchner, A. N. Yaresko, A. Varykhalov, R. Follath, W. Eberhardt, L. Patthey, and H. Berger, *Phys. Rev. Lett.* **102**, 166402 (2009).
- [9] A. Sacchetti, E. Arcangeletti, A. Perucchi, L. Baldassarre, P. Postorino, S. Lupi, N. Ru, I. R. Fisher, and L. Degiorgi, *Phys. Rev. Lett.* **98**, 026401 (2007).
- [10] V. Brouet, W. L. Yang, X. J. Zhou, Z. Hussain, R. G. Moore, R. He, D. H. Lu, Z. X. Shen, J. Laverock, S. B. Dugdale, N. Ru, and I. R. Fisher, *Phys. Rev. B* **77**, 235104 (2008).
- [11] A. Tomeljak, B. Kavcic, H. Schäfer, V. Kabanov, D. Mihailovic, D. Staresinic, K. Biljakovic, and J. Demsar, *Physica B: Condensed Matter* **404**, 548 (2009).
- [12] C. W. Nicholson, C. Berthod, M. Puppini, H. Berger, M. Wolf, M. Hoesch, and C. Monney, *Phys. Rev. Lett.* **118**, 206401 (2017).

- [13] M.-H. Whangbo, E. Canadell, P. Foury, and J. P. Pouget, *Science* **252**, 96 (1991), <https://www.science.org/doi/pdf/10.1126/science.252.5002.96>.
- [14] J. Laverock, S. B. Dugdale, Z. Major, M. A. Alam, N. Ru, I. R. Fisher, G. Santi, and E. Bruno, *Phys. Rev. B* **71**, 085114 (2005).
- [15] M. Calandra and F. Mauri, *Phys. Rev. Lett.* **106**, 196406 (2011).
- [16] H. Luo, Q. Gao, H. Liu, Y. Gu, D. Wu, C. Yi, J. Jia, S. Wu, X. Luo, Y. Xu, L. Zhao, Q. Wang, H. Mao, G. Liu, Z. Zhu, Y. Shi, K. Jiang, J. Hu, Z. Xu, and X. J. Zhou, *Nature Communications* **13**, 273 (2022).
- [17] D. Jérôme, T. M. Rice, and W. Kohn, *Phys. Rev.* **158**, 462 (1967).
- [18] H. P. Hughes, *Journal of Physics C: Solid State Physics* **10**, L319 (1977).
- [19] K. Zhang, X. Liu, H. Zhang, K. Deng, M. Yan, W. Yao, M. Zheng, E. F. Schwier, K. Shimada, J. D. Denlinger, Y. Wu, W. Duan, and S. Zhou, *Phys. Rev. Lett.* **121**, 206402 (2018).
- [20] V. N. Strocov, M. Shi, M. Kobayashi, C. Monney, X. Wang, J. Krempasky, T. Schmitt, L. Patthey, H. Berger, and P. Blaha, *Phys. Rev. Lett.* **109**, 086401 (2012).
- [21] M. D. Johannes and I. I. Mazin, *Phys. Rev. B* **77**, 165135 (2008).
- [22] G. Gruner, ed., *Density Waves In Solids* (CRC Press, 2000).
- [23] A. H. Castro Neto, *Phys. Rev. Lett.* **86**, 4382 (2001).
- [24] A. W. Tsen, R. Hovden, D. Wang, Y. D. Kim, J. Okamoto, K. A. Spoth, Y. Liu, W. Lu, Y. Sun, J. C. Hone, L. F. Kourkoutis, P. Kim, and A. N. Pasupathy, *Proceedings of the National Academy of Sciences* **112**, 15054 (2015).
- [25] M. Hossain, Z. Zhao, W. Wen, X. Wang, J. Wu, and L. Xie, *Crystals* **7** (2017), [10.3390/cryst7100298](https://doi.org/10.3390/cryst7100298).
- [26] H.-H. Kim, E. Lefrançois, K. Kummer, R. Fumagalli, N. B. Brookes, D. Betto, S. Nakata, M. Tortora, J. Porras, T. Loew, M. E. Barber, L. Braicovich, A. P. Mackenzie, C. W. Hicks, B. Keimer, M. Minola, and M. Le Tacon, *Phys. Rev. Lett.* **126**, 037002 (2021).
- [27] Z. Liang, X. Hou, F. Zhang, W. Ma, P. Wu, Z. Zhang, F. Yu, J.-J. Ying, K. Jiang, L. Shan, Z. Wang, and X.-H. Chen, *Phys. Rev. X* **11**, 031026 (2021).
- [28] G. Grüner, *Rev. Mod. Phys.* **60**, 1129 (1988).
- [29] G. Grüner, *Rev. Mod. Phys.* **66**, 1 (1994).
- [30] K. Stolze, A. Isaeva, F. Nitsche, U. Burkhardt, H. Lichte, D. Wolf, and T. Doert, *Angewandte Chemie International Edition*, 862 (2013).

- [31] H. Zhong, C. Bao, T. Lin, F. Wang, X. Cai, P. Yu, and S. Zhou, *Phys. Rev. B* **109**, 165411 (2024).
- [32] F. J. Giessibl, *Rev. Sci. Instr.* **90**, 011101 (2019).
- [33] M. Setvín, J. Javorský, D. Turčinková, I. Matolínová, P. Sobotík, P. Kocán, and I. Ošťádal, *Ultramicroscopy* **113**, 152 (2012).
- [34] F. Huber and F. J. Giessibl, *Rev. Sci. Instrum.* **88**, 073702 (2017).
- [35] M. Schmid, M. Setvín, and U. Diebold, “Device for suspending a load in a vibration-insulated manner,” (2019), uS Patent App. 16/327,528.
- [36] I. Sokolović, M. Schmid, U. Diebold, and M. Setvin, *Phys. Rev. Mater.* **3**, 034407 (2019).
- [37] A. Crepaldi, M. Chergui, H. Berger, A. Magrez, P. Bugnon, F. van Mourik, J. Ojeda, C. A. Arrell, G. Gatti, S. Roth, and et al., *CHIMIA* **71**, 273 (2017).
- [38] A. Janner and T. Janssen, *Phys. Rev. B* **15**, 643 (1977).
- [39] F. D. M. Haldane, *Journal of Physics C: Solid State Physics* **14**, 2585 (1981).
- [40] U. De Giovannini, H. Hübener, S. A. Sato, and A. Rubio, *Phys. Rev. Lett.* **125**, 136401 (2020).
- [41] F. Boschini, M. Zonno, and A. Damascelli, *Rev. Mod. Phys.* **96**, 015003 (2024).
- [42] F. Schmitt, P. S. Kirchmann, U. Bovensiepen, R. G. Moore, L. Rettig, M. Krenz, J.-H. Chu, N. Ru, L. Perfetti, D. H. Lu, M. Wolf, I. R. Fisher, and Z.-X. Shen, *Science* **321**, 1649 (2008).
- [43] J. Maklar, Y. W. Windsor, C. W. Nicholson, M. Puppín, P. Walmsley, V. Esposito, M. Porer, J. Rittmann, D. Leuenberger, M. Kubli, M. Savoini, E. Abreu, S. L. Johnson, P. Beaud, G. Ingold, U. Staub, I. R. Fisher, R. Ernstorfer, M. Wolf, and L. Rettig, *Nature Communications* **12**, 2499 (2021).
- [44] J. Maklar, M. Schüler, Y. W. Windsor, C. W. Nicholson, M. Puppín, P. Walmsley, I. R. Fisher, M. Wolf, R. Ernstorfer, M. A. Sentef, and L. Rettig, *Phys. Rev. Lett.* **128**, 026406 (2022).
- [45] L. Rettig, R. Cortés, J. H. Chu, I. R. Fisher, F. Schmitt, R. G. Moore, Z. X. Shen, P. S. Kirchmann, M. Wolf, and U. Bovensiepen, *Nature Communications* **7**, 10459 (2016).
- [46] G. Gatti, A. Crepaldi, M. Puppín, N. Tancogne-Dejean, L. Xian, U. De Giovannini, S. Roth, S. Polishchuk, P. Bugnon, A. Magrez, H. Berger, F. Frassetto, L. Poletto, L. Moreschini, S. Moser, A. Bostwick, E. Rotenberg, A. Rubio, M. Chergui, and M. Grioni, *Phys. Rev. Lett.* **125**, 076401 (2020).